AKT, NOTCH and GSK3β interact to trigger early myogenesis in vertebrate embryos.

Diane Lebrun[1]*, Pamela Rahal[1]*, Valérie Morin[1], Christophe Marcelle[1,2]

1. Institut NeuroMyoGène (INMG), Université Claude Bernard Lyon1, Faculty of Medicine and Pharmacy, CNRS UMR 5310 - INSERM U1217, Lyon, France
2. Australian Regenerative Medicine Institute (ARMI), Monash University, Clayton, Victoria, Australia,
 *. These authors contributed equally to this work

ABSTRACT

During early embryonic development, migrating neural crest cells expressing the NOTCH ligand Delta1 (DLL1) trigger the activation of NOTCH1 signaling in selected epithelial cells within newly formed somites. A key event in this process is a dramatic inhibition of GSK3β activity, initiated by the activation of NOTCH1 and that takes place independent of its transcriptional function. Here, we investigated the mechanism whereby NOTCH1 exerts its non-canonical function in somites. Using the activation of myogenesis as a read-out of the ability of NOTCH receptors to trigger transcription-independent responses in somites, we found that all NOTCH receptors (1-4) activate MYF5 expression and we showed that the RAM (RBPJ-Associated Molecule) domain of the NOTCH Intracellular Domain (NICD) is necessary and sufficient in this process. We then demonstrated that the NOTCH1 Intracellular Domain (NICD1) physically interacts in the cytosol with GSK3β and with the serine threonine protein kinase AKT. Activating AKT triggers myogenesis, likely via the inhibition of GSK3β. We found that AKT, in a dose-dependent manner, decreases the transcriptional activity of NOTCH, suggesting a role in the balance between the canonical and non-canonical functions of NOTCH. Altogether these data strongly support the hypothesis that transcription-independent function of NICD is a central mechanism driving myogenesis in early somites and suggests that, in this tissue, AKT, NOTCH and GSK3β interact in the cytoplasm to trigger a signaling cascade that leads to the formation of the early myotome in vertebrates.

INTRODUCTION

During early embryogenesis, extensive tissue rearrangements and cell migration, associated with rapid cell fate changes, allow the formation of the tissues and organs of the future adult. A model where such complex issues are amenable to experimentation is the early formation of skeletal muscles in the chick embryo. Over many days of development, the medial border of the dermomyotome (DML) generates the first skeletal muscle cells that assemble into a primary myotome. This arises from a crucial cell fate decision: epithelial cells in the DML either self-renew or undergo myogenic differentiation, accompanied by an epithelial to mesenchymal transition (EMT) that allows their translocation into the primary myotome[1–4].

We previously demonstrated that the activation of MYF5 and MYOD in the DML is dependent upon the transient activation of NOTCH signaling, itself triggered by a mosaic expression of Delta1-positive neural crest cells migrating from the dorsal neural tube, a

47　mode of signaling we named "kiss-and-run" mechanism[4]. The molecular response that
48　takes place within DML cells upon activation by neural crest cells was recently
49　characterized[5]. Within DML cells, the "kiss-and-run" mechanism triggers a signaling
50　module encompassing NOTCH, GSK-3β, SNAI1 and β-catenin and which couples the
51　initiation of myogenesis in DML cells with their EMT (Figure 1A).
52　In the vast majority of cellular processes, NOTCH utilizes a well-characterized
53　"canonical" pathway initiated by the interaction of NOTCH with cell bound ligands
54　(Delta-like or Jagged). This results in cleavage of NOTCH extracellularly by ADAM
55　proteases, and intracellularly by the γ-secretase complex. This releases NICD, which
56　translocates into the nucleus to interact with RBPJ, converting it into a potent
57　transcriptional activator of downstream target genes[6,7]. One of the remarkable features of
58　the kiss-and-run signaling was that the activation of myogenesis by NOTCH seemed
59　independent of its transcriptional function. This was based on the observation that a
60　membrane-tethered NOTCH Intracellular Domain (NICD) displayed similar activity on
61　myogenesis than NICD, while constitutively active and dominant negative forms of the
62　NOTCH effector RPBJ had no effect on this process (Figure 1A). This led to the
63　hypothesis that unconventional functions of NOTCH triggers early myogenesis[5]. Ligand-
64　and transcription-independent functions of NOTCH have been reported in a growing
65　number of cellular contexts and are collectively referred to as "non-canonical" NOTCH
66　signaling[8–10]. NOTCH and WNT/β-catenin signaling are in fact known to interact through
67　non-canonical mechanisms during development and in pathological processes, but in all
68　cases studied, both pathways act antagonistically[11–15]. In contrast, we found that NOTCH
69　promotes the β-catenin-dependent activation of myogenesis in early somites, suggesting
70　that an atypical interaction is at work between these two major signaling pathways to
71　initiate the myogenic program in developing somites.
72　To decipher the molecular events taking place downstream of NOTCH activation, we
73　have now focused our attention on the mechanism inhibiting GSK-3β function. We
74　demonstrated that *in vivo*, NICD, GSK3β and AKT work within a complex, in which
75　AKT kinase activity is required to induce MYF5 expression, likely through its inhibitory
76　role on GSK3β. Reinforcing this hypothesis, we found that SNAI1, a direct target of
77　GSK3β, is a necessary step downstream of AKT in the chain of molecular events leading
78　to myogenesis initiation. We present compelling evidence showing that NICD, GSK3β
79　and AKT interact in the cytosol, suggesting a transcription-independent, non-canonical
80　function of NOTCH in this cellular context. We observed that AKT negatively regulates
81　NOTCH transcriptional activity, suggesting that the canonical and non-canonical
82　NOTCH responses are mechanistically linked. Finally, we uncovered that all NOTCH
83　receptors are able to activate MYF5 expression and we show that the RAM domain of
84　NICD is necessary and sufficient in this process. Altogether these data shed a novel light
85　on the molecular mechanisms whereby NOTCH regulates early myogenic differentiation
86　in vertebrates and suggests that such signaling module could be active in a number of
87　cellular contexts.
88

89　**RESULTS**
90　**All four NOTCH receptors are capable of activating MYF5 expression**
91　There are four NOTCH receptors in the mouse genome, while only three have been
92　detected in the chicken genome[7,16]. Since all receptors share similar canonical functions

93 (e.g. complex formation with the transcription factor RBPJ), it is plausible that they could
94 also share non-canonical, cytoplasmic activities when placed in similar cellular contexts.
95 We speculated that the electroporation of early somites could serve as an experimental
96 paradigm where this hypothesis could be tested. NOTCH1 was previously identified as
97 the endogenous receptor responsible for triggering MYF5 (and MYOD) expression in the
98 DML of chicken embryos through a transcription-independent mechanism[4]. We therefore
99 used the induction of MYF5 expression as a read-out of the ability of other NOTCH
100 receptors to display similar non-canonical functions. We electroporated the constitutively
101 active forms of all four mouse NOTCH (mNICD1-4) in newly formed somites (Figure
102 1B). The chicken NICD1 (cNICD1) served as positive control while the electroporation
103 vector alone (H2B-RFP) served as negative control (indicative of MYF5 expression in
104 normal condition). Six hours later, we analyzed those embryos and we compared the
105 expression of MYF5 in the DML of embryos electroporated with these constructs to that
106 of wild type (WT) embryos. We observed that all four NICD induced a robust activation
107 of MYF5 expression (very similar to that of cNICD1, Figures 1C-D), compared to
108 controls. These data indicate that all NICDs share the same ability to activate
109 myogenesis, likely through the signaling module that we previously uncovered,
110 supporting the assumption that all NOTCH receptors are capable of displaying non-
111 canonical function in specific cellular contexts.
112
113 **The RAM domain is necessary and sufficient for myogenic activation**
114 We then determined which of the domains of NICD is responsible for its non-canonical
115 function. NICD is composed of several domains, including the RAM (RBPJ Associated
116 Module) domain, the 7 Tandem Ankyrin-like Repeats (ANK), the TAD (Trans-Activation
117 Domain) and the PEST domain (Figure 2A[17]). The RAM domain and ANK repeats are
118 thought to be necessary for NOTCH signaling through the canonical (RBPJ-dependent)
119 pathway[18,19]. The RAM domain presents high binding affinity for RBP-J and the ANK
120 domain a low binding affinity for this molecule[20,21]. Since both domains are implicated in
121 protein-protein interactions, we wondered whether they could be involved in the
122 molecular events leading to the induction of myogenesis in the cytosol of DML cells.
123 Since the TAD domain is not present in mNICD4 (Figure 1A), while this molecule is
124 capable of triggering myogenesis (see above), this excluded a role of TAD in early
125 myogenesis. To test the function of the RAM and ANK domains, deletion constructs for
126 each or both domains were generated and electroporated in DML cells of early chicken
127 embryos (Figure 2A). Expression of MYF5 served as a read-out of their activity. As
128 shown in Figures 2B and C, the deletion of the RAM domain significantly decreased the
129 number of MYF5$^+$ electroporated cells as compared to the WT NICD. In contrast, the
130 deletion of the ANK repeats resulted in a percentage of MYF5$^+$ electroporated cells
131 similar to that obtained with the WT NICD. Finally, RAM and ANK deletion presented a
132 significant decrease in MYF5$^+$ cells, similar to that observed in the RAM-only mutant
133 (Figures 2B-C).
134 Since we had previously shown that NICD or a membrane tethered NICD (CD4-NICD)
135 comparably activate MYF5 expression in DML cells[5], we tested whether the same would
136 apply to the NICD deletion mutants. We have shown previously that the fusion of CD4 to
137 NICD results in a molecule that does not enter the nucleus and is unable to activate
138 NOTCH reporters[5]. We found that the deletion of the RAM domain from the CD4-NICD

139 abrogated the induction of MYF5 expression observed after electroporation of the CD4-
140 NICD alone. On the contrary, the deletion of the ANK repeats had no effect (Figure 2 -
141 figure supplement 1 A-C). Together these results suggest that the RAM domain of NICD
142 is necessary for activation of myogenesis in the cytosol of DML cells of the chicken
143 embryo.
144 We next determined whether the RAM domain is sufficient to induce MYF5 expression
145 in DML cells. To demonstrate this, we constructed a plasmid that encodes only the RAM
146 domain (Figure 2A) and we electroporated it in DML cells. We observed that, compared
147 to non-electroporated control embryos, the RAM domain was sufficient to increase the
148 percentage of MYF5$^+$ cells to a similar level to that observed after electroporation of the
149 WT NICD (Figures 2D-E).
150 Altogether, these results suggest that the RAM domain of NICD is necessary and
151 sufficient to trigger the chain of molecular events leading to the induction of myogenesis
152 in the chicken embryo. Since we have shown previously that RBPJ is not involved in
153 myogenesis in the DML[5], this suggests that the RAM domain of NICD likely interacts
154 with other protein(s) to mediate its pro-myogenic activity.
155
156 **NICD physically interacts with GSK3β and AKT in the cytoplasm of muscle**
157 **progenitors.**
158 Using a reporter for GSK-3β activity, we have previously shown that both NICD and a
159 membrane-tethered CD4-NICD induce a dramatic inhibition of GSK-3β activity[5].
160 Although previous studies suggested that GSK-3β binds to NOTCH to activate or inhibit
161 its transcriptional activity[22,23], the mechanism whereby NOTCH could regulate GSK-3β
162 activity is unknown. As a first step towards this aim, we tested whether NICD and GSK-
163 3β physically interact *in vivo*. We performed co-immunoprecipation (co-IP) experiments
164 on total protein extracts of somites electroporated with tagged (myc) NICD and CD4-
165 NICD. We analyzed the embryos six hours after electroporation. This focuses on primary
166 events resulting from expression of the constructs. About 40-50 electroporated embryos
167 per condition were tested and the experiments were repeated 3 times. Protein extracts
168 (1mg/lane) showed equivalent amounts of GAPDH protein in all samples (Figure 3A).
169 Similar amounts of endogenous GSK-3β protein were also present in all protein extracts
170 and the electroporated constructs (NICD and CD4-NICD) were also detected. Analysis of
171 the immunoprecipitates showed that NICD and CD4-NICD co-precipitated
172 GSK3β (Figure 3B). Quantification of three independent co-IPs suggests that NICD
173 physically interacts with GSK3β in muscle progenitors present within the DML (Figure
174 3C). The observation that the NICD and the membrane-tethered NICD (CD4-NICD) co-
175 precipitated GSK-3β, suggests that the physical interaction between NICD and GSK3β is
176 taking place in the cytosol.
177 Since NICD does not display any kinase activity to inhibit GSK-3β, it is unlikely that
178 NICD directly regulates GSK-3β activity. Therefore, it is probable that another kinase(s)
179 is responsible for this effect. A well-documented GSK-3β modulator is the serine
180 threonine kinase AKT (also known as Protein Kinase B)[24–26], which phosphorylates and
181 inhibits GSK-3β, notably in response to growth factor stimulation or to G-protein-
182 coupled receptor (GPCR) activation.
183 We first determined whether AKT is co-expressed with NOTCH when myogenesis is
184 first initiated in developing embryos, i.e. in the medial border of the dermomyotome of

4

185   newly formed somites (DML)[4]. As in mammals, 3 AKT homologs (1-3) are present in the
186   chicken genome. We performed in situ hybridization with probes for AKT1-3 on
187   developing embryos and we observed that AKT1 is expressed in the DML at the time that
188   muscle progenitors are generated in this structure, supporting the possibility that this
189   molecule could play a role in this process (Figure 3 - figure supplement 1 A-B). This
190   observation is coherent with data in mice, where AKT1 was found to be the main AKT
191   expressed during embryonic development[27].
192   In the somite extracts electroporated with the two NICD variants described above, we
193   observed that endogenous AKT co-precipitated with NICD and CD4-NICD, suggesting
194   that NICD and AKT proteins physically interact within the cytosol of DML cells (Figures
195   3A-C).
196   Together these results show that NICD directly interacts with GSK3β and AKT at the
197   initial step of the signaling cascade leading to myogenesis. Furthermore, given the
198   reported inhibitory role of AKT on GSK3β, our results suggest that AKT mediates the
199   GSK3β inhibition needed to trigger the signaling cascade for induction of myogenesis in
200   the DML.
201
202   **AKT induces MYF5 expression in a kinase-dependent manner.**
203   If AKT were to inhibit GSK3β in the DML, modulating its activity should affect
204   myogenesis. To test this we electroporated the DML of developing chicken embryos with
205   a construct coding for a wild type or a constitutively active form of AKT (CA AKT).
206   Quantification of the proportion of electroporated cells expressing MYF5 showed that
207   both WT and CA AKT expression led to a robust increase in the proportion of MYF5-
208   positive cells (Figures 4A-B). This increase was alike the effect obtained after NICD
209   over-expression in DML cells (see above and[4]). To verify that the kinase domain is
210   required for this effect we electroporated a kinase-dead form of AKT. In this case, the
211   number of MYF5-positive cells was comparable to control embryos. Altogether, these
212   data suggest that the kinase activity of AKT controls the activation of MYF5 expression
213   in the DML.
214
215   **AKT regulates myogenesis through SNAI1**
216   The result above is coherent with the hypothesis that AKT acts on GSK3β. However,
217   AKT is a pleiotropic kinase with a multitude of known substrates. Therefore, it is
218   possible that the activation of MYF5 expression we observed after activation of AKT was
219   only partly due to its activity on GSK3β. To address this possibility, we tested whether
220   blocking a downstream target of GSK3β would counteract the AKT-mediated activation
221   of MYF5. A direct consequence of GSK3β inhibition in muscle progenitors is a
222   stabilization of the transcription factor Snail1 (SNAI1)[5]. SNAI1 is a direct target of
223   GSK3β[28] and SNAI1 stabilization is a necessary step for activation of MYF5 in the
224   DML[5]. We have co-electroporated AKT, together with a dominant-negative form of
225   SNAI1 (DN SNAI1[5,29]). We observed that the increase in MYF5 expression observed
226   with AKT alone was abrogated when DN SNAI1 was co-expressed with AKT (Figures
227   5A-B). This confirms SNAI1 activation is a necessary step downstream of AKT-
228   mediated MYF5 expression, and altogether reinforces the hypothesis that, within the time
229   frame of these experiments, AKT regulates GSK3β activity in the DML.
230

AKT, independent of its kinase activity, negatively regulates NOTCH transcriptional function

The data above strongly suggest that AKT is a novel component of the signaling module, upstream of SNAI1, which translates the activation of NOTCH by migrating DLL1-positive neural crest cells into an initiation of the myogenic program in DML cells. To test whether AKT may also regulate the canonical function of NOTCH, we co-electroporated increasing amounts of a tagged form of AKT together with a NOTCH reporter[4]. We observed that the activity of the reporter decreased with the increasing quantity of AKT (Figures 6A-B). The decrease in NOTCH transcriptional activity is likely independent of AKT kinase activity, since the co-electroporation of a dominant-negative (DN, i.e. kinase-dead) and a constitutively active mutant forms of AKT led to a similar decrease in the NOTCH reporter activity (Figures 6C-D). Finally, we found that the NOTCH transcriptional activity was similarly decreased when membrane-tethered forms of AKT and DN AKT were electroporated in DML cells (Figures 6E-F). Altogether, these data suggest that the balance between the transcriptional and non-transcriptional activities of NOTCH is mechanistically linked in DML cells. The mechanism whereby this regulation may take place is yet to be uncovered, but our data suggest that it may be due to an interaction between NICD and AKT that takes place in the cytosol.

DISCUSSION

The purpose of this study was to characterize the mechanism whereby NOTCH plays non-canonical (ligand-dependent, but transcription-independent) functions in the DML. The demonstration that NOTCH, AKT and GSK3β physically interact in the cytosol of DML cells provides direct evidence for a role of NICD in the cytoplasm of those cells (Figure 7). It also identifies the binding of GSK3β to NOTCH as the initiating event, immediately downstream of NOTCH activation by incoming neural crest cells, in the signaling module leading to the initiation of MYF5 expression in this tissue.

The identification of AKT in a protein complex with NOTCH suggests a possible mechanism whereby NOTCH could inhibit GSK3β activity: GSK3β being a major target of AKT[24–26], it is tempting to postulate that its activity is inhibited by AKT within a protein complex encompassing all three molecules. AKT is a pleiotropic kinase that acts on a number or targets in various cellular contexts. In muscles, AKT is a major regulator of muscle mass through the mTOR and FoxO anabolic and catabolic pathways[30]. However, the observation that SNAI1 activation is a necessary step downstream of GSK3β and AKT supports a model whereby, within the short time frame of our experiments in DML cells, AKT regulates myogenesis solely through its action on GSK3β (Figure 7).

Interestingly, it was shown that the phosphorylation of NOTCH by GSK3β positively regulates canonical (transcriptional) NOTCH signaling *in vitro*[23]. It is thus possible that this explains the decrease in NOTCH transcriptional activity we observed with increasing AKT concentration (Figure 6). AKT and GSK3β would then act as molecular switches between canonical and non-canonical NOTCH signaling.

AKT is itself activated by the stimulation of receptor tyrosine kinases (RTK) or G-protein-coupled receptors (GPCR). Binding to their cognate ligand leads to plasma membrane recruitment and activation of the phosphoinositide 3-kinase (PI3K) that in turn

6

277 activates AKT[31]. The uncovering that AKT plays a role in the signaling module
278 triggering myogenesis therefore suggests that additional inputs from RTKs and/or GPCRs
279 into the pathway leading to the activation of the myogenic program may play a role
280 during this process. The nature of this signal(s) is only speculative at this point. Many
281 FGFs (which signal through FGFR1-4 RTKs) are robustly expressed by the growing
282 myotome, directly adjacent to the DML[29]. Frizzled (GPCR) that transduce WNT signals
283 carried by migrating neural crest cells or secreted by the overlaying ectoderm are also
284 present in the DML[3,5,32,33]. It was also suggested that Sonic Hedgehog (SHH, whose role
285 in early myogenesis has been debated[34]) activates AKT phosphorylation[35,36]. Whether in
286 the DML SHH, FGFs, WNTs or other signals synergize with NOTCH signaling *via* AKT
287 to trigger early myogenic differentiation remains to be shown (Figure 7).
288 Finally, the observation that the NICDs of all four NOTCH receptors similarly activate
289 myogenesis in the DML strongly suggests that they do so through similar, non-canonical
290 mechanisms. The widespread expression of AKT, GSK3β and the NOTCH receptors
291 suggests that similar interactions between those molecules could take place in many
292 cellular contexts where cell fate changes are associated with an EMT.
293 Since NOTCH is such an extensively studied molecule, it may seem surprising that such
294 interaction of NOTCH with widely expressed kinases was never reported. It is possible
295 that the experimental paradigm we are using (analyses of tissues 2-3 hours after
296 constructs initiate expression) allows detecting events immediately downstream of
297 NOTCH activation that could have gone un-noticed with longer-term approaches. Our
298 finding does not exclude a canonical role for NOTCH. In fact we have shown that in
299 somites, NICD also enters the nucleus where it presumably triggers transcription together
300 with RBPJ[4,5]. However, the phenotypical consequences of its nuclear functions in this
301 tissue are unknown.
302 In conclusion, this study provides novel evidence for a transcription-independent function
303 for NICD in somites and establishes AKT as a novel key player in the signaling cascade
304 that leads to the formation of the early myotome in vertebrates
305
306 **MATERIAL AND METHODS**
307 **Electroporation**
308 The somite electroporation technique that was used throughout this study has been
309 described elsewhere[2–4,37]. Briefly, we targeted the expression of various constructs to the
310 dorso-medial portion of newly formed interlimb somites of Hamburger–Hamilton (HH[38])
311 stage 15–16 chick embryos (24–28 somites). We have previously shown that this
312 technique allows the specific expression of cDNA constructs in the DML, and that
313 fluorescent reporters (e.g. GFP) are detected 3 hr after electroporation in this structure[39].
314 We have analyzed all embryos 6 hrs after electroporation, implying that the molecules
315 under study here have been acting during a narrow timeframe (about 3 hrs).
316
317 **Expression constructs**
318 *The following constructs have been previously published:*
319 The CAGGS-H2B–RFP (provided by Dr. S. Tajbakhsh[4]) contains a fusion of Histone 2B
320 with RFP, downstream of the CAGGS strong ubiquitous promoter (CMV/chick β-actin
321 promoter/enhancer).

322 The CAGGS–EGFP[4] contains the CAGGS promoter followed by the EGFP reporter
323 gene.
324 The dominant negative form of SNAI1 consists of the chicken SNAI1, in which the
325 repressor domain was replaced by the VP16 activator domain of the Herpes simplex
326 virus[29].
327 CAGGS HA-NICD-6xMyc contains the chicken NICD1 (aa 1763-2561) of the chicken
328 NOTCH1, flanked with HA and 6xMyc downstream of the CAGGS promoter[4].
329 The GSK3 biosensor (pCS2 GFP-GSK3-MAPK, Addgene #29689) contains a CMV
330 promoter upstream of a GFP molecule followed by a polypeptide tail that contains 3
331 GSK-3β phosphorylation sites, a priming site for MAPK/Erk and a site for the binding of
332 E3 polyubiquitin ligases[40].
333 HES1–d2EGFP (provided by Dr. R. Kageyama) contains the HES1 mouse promoter
334 followed by a destabilized d2EGFP[41].
335 The membrane tagged NICD was constructed using Gibson assembly (NEB) with the
336 signal peptide FGFR2 (from *Danio rerio*), the extracellular and transmembrane domain
337 of human CD4 (both obtained from Dr. J Kaslin) followed by the HA tagged NICD
338 previously described, cloned either into the bidirectional vector tetracycline responsive
339 vector or into the pCX-Myc described above.
340 The H2B-BFP has been made by replacing the RFP from the CAGGS-H2B–RFP
341 described above by a TagBFP (Evrogen) [5].
342 CAGGS-BFP has been made by cloning the TagBFP (Evrogen) into the pCAGGS vector.
343   *The following plasmids were constructed:*
344 The four mouse NICD have been made by cloning them (addgene 20183, 20184, 20185
345 and 20186) using Gibson simple fragment assembly with pCAAGS HA-NICD-6xMYC
346 (described in[4]) as a backbone, opened with ClaI and BglII restriction enzymes.
347
348 The deletion mutants of the cNICD1 and the RAM domain have been constructed
349 according to the description domains[42], by deletion of the pCAAGS HA-NICD described
350 in[5] with a Gibson double fragment assembly with the XbaI enzyme.
351
352 The delta CD4-NICD have been constructed as the delta NICD, using the pCAAGS CD4
353 HA-NICD-6xMYC[5] as a backbone. The CD4 membrane-tethering tail contains the signal
354 peptide FGFR2 (from *Danio rerio*), followed by the extracellular and transmembrane
355 domain of human CD4 (both obtained from Dr. J. Kaslin).
356
357 The AKT variants have been constructed by Gibson simple fragment assembly with
358 pCAAGS HA-NICD-6xMyc described in[4] as a backbone, open with ClaI and EcoRI. The
359 AKT variants were obtained from addgene 39531, 16243 and 17245.
360
361 The CD4-AKT variants have been constructed as the AKT variants, using the pCAAGS
362 CD4 HA-NICD-6xMYC[5] as a backbone.
363
364 **Immunohistochemistry, in situ hybridization.**
365 Whole-mount antibody staining was performed as described[3]. The following antibodies
366 were used: rabbit polyclonals directed against chick myogenic regulatory factor MYF5
367 (obtained from Dr. B. Paterson[43]; 1/200); and anti-RFP (Abcam #62341, 1/1000); chicken

8

368 polyclonal antibody against EGFP (Abcam #13970, 1/1000). Mouse monoclonal
369 antibodies against c-myc-tag (Abcam #32072, 1/200), HA-tag (CST, #2367S, 1/100). In
370 situ hybridization was performed as described[29]. Probes for AKT1, 2 and 3 were isolated
371 by RT-PCR of total RNA extracted from chicken embryonic E19 brain and E14 muscle
372 tissues mixed together. The primers designed for amplification were derived from
373 GenBank chicken AKT1-3 sequences. Amplified fragments (about 600 bp each) were
374 cloned into the pGEM-T vector and sequence-verified.
375
376 **Confocal analyses**
377 Dorsal views of somites shown in all figures are projections of stacks of confocal images
378 taken using a 4-channel Leica SP5 confocal microscope (Leica). Confocal stacks of
379 images were visualized and analyzed with the Imaris software suite (Bitplane). Cell
380 counting was performed using the cell counter plugin (Kurt De Vos, University of
381 Sheffield) within the ImageJ software[44].
382
383 **Quantifications and statistical analyses**
384 Electroporation results in the transfection of a portion of the targeted cell population,
385 which is variable from embryo to embryo. To precisely evaluate the phenotypes obtained
386 after electroporation of cell-autonomously acting cDNA constructs, the number of
387 positive cells was compared to the total number of electroporated cells, recognized by an
388 internal fluorescent reporter construct. On average, more than 700 cells were counted per
389 point and the corresponding quantifications are shown in all figures.
390 To determine the fluorescence intensity of electroporated cells, the surface of
391 electroporated cells were rendered manually with Imaris software. The mean intensity for
392 each cell and each channel in three-dimensions was collected for statistical analyses.
393 Statistical analyses were performed using the GraphPad Prism software. Mann–Whitney
394 non-parametric two-tail testing was applied to populations to determine the P values
395 indicated in the figures. In each graph, columns correspond to the mean and error bars
396 correspond to the standard deviation. ***p value < 0.001, extremely significant; **p
397 value 0.001 to 0.01, very significant.
398
399 **Co-Immunoprecipitation**
400 Two and a half day old non-electroporated (WT) chick embryos or embryos
401 electroporated in the DML with HA-NICD-6xcMyc (NICD) or HA-CD4-NICD-6xcMyc
402 (CD4-NICD) were incubated for 6hrs at 37°C. After screening, somites of approximately
403 40 embryos per condition containing electroporated (NICD and CD4-NICD) and non-
404 electroporated (WT) DML cells were mechanically dissected under the microscope,
405 homogenized using 26 gauge syringes and lyzed for 1h at 4°C using lysis buffer present
406 in the coIP kit (Active Motif Co-IP kit). Cell Lysates were then centrifuged for 10min at
407 4°C at 14000 rpm and supernatants were dosed using Bio-Rad DC protein assay (DC
408 protein assay kit, Bio-Rad, 500-0116). Cell lysates were subjected to co-IP experiment as
409 described by Active Motif universal Magnetic coIP Kit (ref: 54002). Briefly, 1mg of total
410 protein extracts were incubated with c-Myc antibody O/N at 4°C. The next day, 30uL of
411 Magnetic beads were added to the mix and incubated for 1hr at 4°C. Negative control
412 consists of NICD or CD4-NICD electroporated lysates with only magnetic beads
413 addition. Afterward, beads were collected using a magnetic stick and supernatants were

9

414   removed. The beads were washed for up to 5 times using the Co-IP/ wash Buffer in the
415   Kit. Lastly, beads were resuspended with 2X Laemmli loading buffer and heated for
416   10min at 95°C before migration on a 10% SDS-page gel and transfer into a PVDF
417   membrane (Millipore, IPVH00010) for western blot analysis.
418
419   **Western blot**
420   For co-IP inputs lanes, 30 μg of total protein extract samples and co-IP eluates
421   resuspended with 2x Laemmli buffer were separated on a 10% SDS-PAGE gel, then
422   transferred onto PVDF Immobilon-P membranes (Millipore, IPVH00010). After
423   transfert, membranes were blocked with 5% of non-skimmed milk diluted in TBS-T
424   (Tris-buffered saline (50 mM Tris, 150 mM NaCl, pH 7.4) + 0.1% Tween 20) and
425   incubated overnight at 4°C with 1/1000 diluted primary antibodies including c-Myc
426   (abcam; ab-32), GSK3β (cell signaling technology; cs-9832), AKT (cell signaling
427   technology; cs-9272S) and GAPDH (cell signaling technology; cs-2118). Membranes
428   were washed 3 times in TBS-T for 15 min and incubated for 1hour at RT with
429   horseradish peroxidase-conjugated secondary antibodies (1/10 000). After 3 washes of 5
430   minutes each in TBS-T, membranes were incubated with enhanced chemiluminescence
431   reagents (Amersham ECL Prime, GE Healthcare; Ref: RPN2232) and revealed by
432   Chemiluminescence detecting machine from Thermo Electron Corporation (serial
433   number: 392-562L (RS232C)).
434
435
436

10

FIGURE LEGENDS

Figure 1: all NOTCH receptors activate MYF5 expression. (**A**) A simplified model representing the sequence of molecular events taking place at the DML during early myogenesis (adapted from [5]). Delta1 (DLL1) from migrating neural crest cells (NC) activates NOTCH receptor in DML cells. The inhibition of GSK3β by NICD leads to the stabilization of Snail1 (SNAI1), which in turn triggers an EMT. As a consequence, β-catenin from the adherens junction (AJ) enters the nucleus where it activates myogenesis (**B**) Structure of the intracellular domains (NICDs) of the mouse NOTCH receptors (1-4) and of the chicken NICD1. All NICD constructs are tagged to allow detection (not shown). Indicated sizes are without the HA and Myc tags. (**C**) Confocal stacks of somites 6h after electroporation of the four mouse NICD isoforms, immunostained for c-myc (in green) and RFP (in red) to detect the electroporation marker (H2B-RFP). MYF5 expression is shown in blue. Dotted lines delineate the borders of the DML. (**D**) bar chart showing the percentage of electroporated MYF5$^+$ cells compared to the total number of electroporated cells. ***:P<0,001 31,7% of cells electroporated with the electroporation marker express MYF5; 78,7% the cells electroporated with the chicken NICD express MYF5 and respectively 76,2%, 77,5%, 77,6% and 75,1% of the cells electroporated with the isoforms 1 to 4 of the mouse NICD express MYF5. Scale bar: 50μm

Figure 2: the NICD RAM domain is necessary and sufficient to induce Myf5 expression. (**A**) Schematics of the NICD mutants used in this experiments. All NICD constructs are tagged to allow detection (see Material and Methods). Size of cNICD1 (912 aa) takes the HA and Myc tags into account. Amino acid numbering is derived from the chicken NOTCH 1 (GenBank accession # XP_015134811.1). (**B**) Confocal stacks of somites 6h after electroporation of mutant forms of cNICD1 (in green) together with an electroporation marker (in red). MYF5 expression is shown in blue. (**C**) Bar charts showing the percentage of electroporated MYF5$^+$ cells. 28,0% of electroporated cells express MYF5 in controls, 71,9% with NICD and 36,7%, 71,9, and 41,4% with a NICD missing the RAM domain, the ANK domain, and both the RAM and ANK domains, respectively. (**D**) Confocal stacks of somites after electroporation of either cNICD1 or the RAM domain of cNICD1 (in green), together with an electroporation marker (in red). MYF5 expression is shown in blue. (**E**) Bar charts showing the percentage of electroporated MYF5$^+$ cells. 29,0% of electroporated cells express MYF5 in controls, 79,0% with chicken NICD and 80,8% with the RAM domain only. ***:p<0,001. Scale bars: 50μm. Dotted white lines indicate the borders of the dorsomedial lip of the somite. Scale bars: 50μm

Figure 3: NICD physically interacts with GSK3β and AKT in the cytoplasm of muscle progenitors. Co-IP of endogenous GSK3β and AKT by exogenously expressed, tagged NICD and membrane tethered (CD4-)NICD. (**A**) Detection of GSK3β and AKT in total protein extracts (1mg) of DML electroporated with controls (WT), NICD and CD4-NICD plasmids. (**B**) 30 μg of the protein extract were used for coIP with c-Myc antibody and reacted with GSK3β and AKT antibodies (for AKT, we used an antibody that recognizes all 3 AKTs). Negative control lane is a test of the co-IP beads specificity: NICD electroporated extract, no c-Myc antibody, and reacted with Magnetic coIP beads.

11

482   (**C**) Bar charts representing the results (mesured in bands intensities) of 3 coIP
483   experiments (as shown in B). GSK3β (dark grey) and AKT (light grey).
484

485   **Figure 4: Akt induces myogenesis in a kinase-dependent manner.** (**A**) Confocal stacks
486   of somites 6h after electroporation of NICD or several AKT variants (in red) together
487   with a nuclear electroporation marker (in blue). MYF5 expression is shown in grey. (**B**)
488   Bar chart showing the percentage of electroporated MYF5^{+} cells in the DML. Controls
489   electroporated with the marker (31,0% of electroporated cells express MYF5); 81,9%
490   MYF5^{+} with NICD and 76,8%, 76,9, and 41,7% were MYF5^{+} after electroporation of
491   ATK, Myr-AKT (CA) and DN-AKT. ***: p<0,001. Dotted white lines indicate the
492   borders of the DML. Scale bar: 50μm
493

494   **Figure 5: AKT regulates myogenesis through SNAI1 stabilization.** (**A**) Confocal
495   stacks of somites 6h after electroporation of AKT (in red), a dominant negative form of
496   SNAI1[29] (in green) or both plasmids, together with an electroporation marker (blue).
497   MYF5 is shown in grey. Dotted white lines indicate the borders of the DML. Scale bars:
498   50μm. (**B**) Bar chart showing the % of electroporated MYF5^{+} cells. Controls: 26,0%
499   MYF5^{+}; AKT 71,2% MYF5^{+}; DN-SNAI1, 13,6% MYF5^{+}; AKT & DN-SNAI1, 21,2%
500   MYF5^{+}. ***: p<0,001. Scale bar: 50μm
501

502   **Figure 6: AKT negatively regulates NOTCH transcriptional function, independently**
503   **of its kinase activity.** (**A, C, E**) Confocal stacks of somites 6h after electroporation (in
504   red) of AKT (A,C); a constitutively active form of AKT (CA-AKT) and a dominant
505   negative form of AKT (DN-AKT, C); a membrane-tethered form of AKT (CD4-AKT) or
506   of DN-AKT (CD4-DN-AKT, E). They were co-electroporated with a reporter of NOTCH
507   transcriptional activity (Hes1-GFP[4], in green) and an electroporation marker (in blue).
508   Dotted lines indicate the borders of the DML. Scale bars: 50μm. (**A**) Increasing amounts
509   of AKT. (**C**) Electroporation of AKT, DN-AKT, CA-AKT. (**E**) Electroporation of CD4-
510   AKT or CD4-DN-AKT. (**B**) Bar charts showing the decreasing transcriptional activity of
511   NOTCH with increasing amounts of exogenous AKT. Relative intensities (in U.A.): 1884
512   in controls (no AKT); 1254 with 0,5μg/μL AKT; 937 with 1μg/μL; 517 with 3μg/μL. (**D**)
513   Bar charts showing that 27,1% of DML cells electroporated with AKT express the
514   NOTCH reporter; 26,4% with DN-AKT; 22,0% with CA-AKT; in controls, 48,1% of
515   electroporated cells express the NOTCH reporter. (**F**) Bar charts showing 27,5% NOTCH
516   reporter^{+} cells with CD4-AKT; 25,2% NOTCH reporter^{+} cells with CD4-DN-AKT; and
517   45,7% NOTCH reporter^{+} cells in controls. ***:p<0,001; **: p<0,005. Scale bars: 50μm
518

519   **Figure 7: A model describing the main findings of this study.** Contact between
520   Delta1-positive neural crest and epithelial DML cells trigger the activation of NOTCH
521   receptor in the latter. In the cytosol, this leads to the physical binding of NICD, through
522   its RAM domain, to the serine-threonine kinases AKT and GSK3-β. The result of this
523   interaction is a robust inhibition of GSK3-β, which leads to the stabilization of the EMT
524   master gene SNAI1. AKT is an integral part of the signaling module leading to
525   myogenesis, since it's activation triggers MYF5 expression in a SNAI1-dependent
526   fashion.
527

12

SUPPLEMENTARY FIGURE LEGENDS

Figure 2 - figure supplement 1: A membrane-tethered NICD depleted of its RAM domain is unable to activate Myf5 expression. (**A**) Schematics of the NICD mutants used in this experiments. All NICD constructs are tagged and attached to the membrane by fusion to the transmembrane domain of the human CD4. Indicates size of CD4 NICD1 (1161 aa) takes the tags and the CD4 membrane attachment into account. Amino acid numbering is derived from the chicken NOTCH 1 (GenBank accession # XP_015134811.1). (**B**) Confocal stacks of somites 6h after electroporation of mutant forms of a membrane-tethered (CD4)-NICD (in green), together with an electroporation marker (in blue). MYF 5 expression is in blue. (**C**) Bar charts showing that CD4-NICD and a CD4-NICD deleted of its ANK domain similarly activate MYF5 expression (81% and 77% of electroporated cells are MYF5+, respectively), compared to control embryos (32%). CD4-NICD deleted of its RAM domain or of the RAM and ANK domains are unable to activate MYF5 (36% in both conditions). ***:p<0,001. Scale bar: 50μm

Figure 3 - figure supplement 1: AKT1 is expressed in the DML of chicken somites. (**A,B**) Whole mount in situ hybridization on E 3.5 day old chicken embryos (Hamburger and Hamilton stage 21) with an AKT1-specific probe. Widespread expression is observed throughout the embryo, e.g. the limbs (L), the neural tube (NT) and the somites (S). The DML of all somites expresses Akt1 (arrows). (**B**) is an enlargement that corresponds to the boxed area in A.

ACKNOWLEDGMENTS

REFERENCES

1. Denetclaw, W. F., Christ, B. & Ordahl, C. P. Location and growth of epaxial myotome precursor cells. *Development* **124,** 1601–10 (1997).
2. Gros, J., Scaal, M. & Marcelle, C. A two-Step mechanism for myotome formation in chick. *Dev. Cell* **6,** (2004).
3. Gros, J., Serralbo, O. & Marcelle, C. WNT11 acts as a directional cue to organize the elongation of early muscle fibres. *Nature* **457,** (2009).
4. Rios, A. C., Serralbo, O., Salgado, D. & Marcelle, C. Neural crest regulates myogenesis through the transient activation of NOTCH. *Nature* **473,** (2011).
5. Sieiro, D., Rios, A. C., Hirst, C. E. & Marcelle, C. Cytoplasmic NOTCH and membrane-derived β-catenin link cell fate choice to epithelial-mesenchymal

574   transition during myogenesis. *Elife* **5,** (2016).

575   6.   Kopan, R. & Ilagan, M. X. G. The Canonical Notch Signaling Pathway: Unfolding
576   the Activation Mechanism. *Cell* **137,** 216–233 (2009).

577   7.   Hori, K., Sen, A. & Artavanis-Tsakonas, S. Notch signaling at a glance. *J. Cell Sci.*
578   **126,** 2135–2140 (2013).

579   8.   Ayaz, F. & Osborne, B. A. Non-Canonical Notch Signaling in Cancer and
580   Immunity. *Front. Oncol.* **4,** (2014).

581   9.   Andersen, P., Uosaki, H., Shenje, L. T. & Kwon, C. Non-canonical Notch
582   signaling: Emerging role and mechanism. *Trends in Cell Biology* **22,** 257–265
583   (2012).

584   10.   D'Souza, B., Meloty-Kapella, L. & Weinmaster, G. *Canonical and non-canonical*
585   *notch ligands*. *Current Topics in Developmental Biology* **92,** (2010).

586   11.   Collu, G. M. *et al.* Dishevelled limits Notch signalling through inhibition of CSL.
587   *Development* **139,** 4405–4415 (2012).

588   12.   Kwon, C. *et al.* Notch post-translationally regulates beta-catenin protein in stem
589   and progenitor cells. *Nat Cell Biol* **13,** 1244–1251 (2011).

590   13.   Acosta, H., Lopez, S. L., Revinski, D. R. & Carrasco, A. E. Notch destabilises
591   maternal -catenin and restricts dorsal-anterior development in Xenopus.
592   *Development* **138,** 2567–2579 (2011).

593   14.   Munoz-Descalzo, S., Tkocz, K., Balayo, T. & Arias, A. M. Modulation of the
594   ligand-independent traffic of Notch by Axin and Apc contributes to the activation
595   of Armadillo in Drosophila. *Development* **138,** 1501–1506 (2011).

596   15.   Sanders, P. G. T. *et al.* Ligand-independent traffic of notch buffers activated
597   armadillo in Drosophila. *PLoS Biol.* **7,** (2009).

598   16.   Bray, S. J. Notch signalling in context. *Nature Reviews Molecular Cell Biology* **17,**
599   722–735 (2016).

600   17.   Lubman, O. Y., Korolev, S. V. & Kopan, R. Anchoring Notch genetics and
601   biochemistry: Structural analysis of the ankyrin domain sheds light on existing
602   data. *Molecular Cell* **13,** 619–626 (2004).

603   18.   Nofziger, D., Miyamoto, A., Lyons, K. M. & Weinmaster, G. Notch signaling
604   imposes two distinct blocks in the differentiation of C2C12 myoblasts.
605   *Development* **126,** 1689–702 (1999).

606   19.   Shawber C *et al.* Notch signaling inhibits muscle cell differentiation through a
607   CBF1-independent pathway. *Development* **122,** 3765–3773 (1996).

608   20.   Tamura, K. *et al.* Physical interaction between a novel domain of the receptor
609   Notch and the transcription factor RBP-J kappa/Su(H). *Curr Biol* **5,** 1416–1423
610   (1995).

611   21.   Roehl, H., Bosenberg, M., Blelloch, R. & Kimble, J. Roles of the RAM and ANK
612   domains in signaling by the C. elegans GLP-1 receptor. *Embo J.* **15,** 7002–7012
613   (1996).

614   22.   Espinosa, L., Inglés-Esteve, J., Aguilera, C. & Bigas, A. Phosphorylation by
615   glycogen synthase kinase-3β down-regulates Notch activity, a link for Notch and
616   Wnt pathways. *J. Biol. Chem.* **278,** 32227–32235 (2003).

617   23.   Foltz, D. R., Santiago, M. C., Berechid, B. E. & Nye, J. S. Glycogen synthase
618   kinase-3beta modulates notch signaling and stability. *Curr. Biol.* **12,** 1006–1011
619   (2002).

24. Cross, D. a, Alessi, D. R., Cohen, P., Andjelkovich, M. & Hemmings, B. a. Inhibition of glycogen synthase kinase-3 by insulin mediated by protein kinase B. *Nature* **378,** 785–9 (1995).

25. Ter Haar, E. *et al.* Structure of GSK3β reveals a primed phosphorylation mechanism. *Nat. Struct. Biol.* **8,** 593–596 (2001).

26. McCubrey, J. A. *et al.* Effects of mutations in Wnt/β-catenin, hedgehog, Notch and PI3K pathways on GSK-3 activity—Diverse effects on cell growth, metabolism and cancer. *Biochimica et Biophysica Acta - Molecular Cell Research* **1863,** 2942–2976 (2016).

27. Yang, Z.-Z. *et al.* Dosage-Dependent Effects of Akt1/Protein Kinase Bα (PKBα) and Akt3/PKBγ on Thymus, Skin, and Cardiovascular and Nervous System Development in Mice. *Mol. Cell. Biol.* (2005). doi:10.1128/MCB.25.23.10407-10418.2005

28. Zhou, B. P. *et al.* Dual regulation of Snail by GSK-3beta-mediated phosphorylation in control of epithelial-mesenchymal transition. *Nat. Cell Biol.* **6,** 931–40 (2004).

29. Delfini, M.-C. *et al.* The timing of emergence of muscle progenitors is controlled by an FGF/ERK/SNAIL1 pathway. *Dev. Biol.* **333,** (2009).

30. Egerman, M. A. & Glass, D. J. Signaling pathways controlling skeletal muscle mass. *Critical Reviews in Biochemistry and Molecular Biology* (2014). doi:10.3109/10409238.2013.857291

31. Manning, B. D. & Toker, A. AKT/PKB Signaling: Navigating the Network. *Cell* **169,** 381–405 (2017).

32. Serralbo, O. & Marcelle, C. Migrating cells mediate long-range WNT signaling. *Dev.* **141,** (2014).

33. Linker, C. *et al.* β-catenin-dependent Wnt signalling controls the epithelial organisation of somites through the activation of paraxis. *Development* **132,** (2005).

34. Münsterberg, A. E., Kitajewski, J., Bumcrot, D. A., McMahon, A. P. & Lassar, A. B. Combinatorial signaling by Sonic hedgehog and Wnt family members induces myogenic bHLH gene expression in the somite. *Genes Dev.* **9,** 2911–2922 (1995).

35. Riobó, N. A., Lu, K., Ai, X., Haines, G. M. & Emerson, C. P. Phosphoinositide 3-kinase and Akt are essential for Sonic Hedgehog signaling. *Proc. Natl. Acad. Sci. U. S. A.* **103,** 4505–10 (2006).

36. Elia, D., Madhala, D., Ardon, E., Reshef, R. & Halevy, O. Sonic hedgehog promotes proliferation and differentiation of adult muscle cells: Involvement of MAPK/ERK and PI3K/Akt pathways. *Biochim. Biophys. Acta* **1773,** 1438–46 (2007).

37. Gros, J., Manceau, M., Thomé, V. & Marcelle, C. A common somitic origin for embryonic muscle progenitors and satellite cells. *Nature* **435,** (2005).

38. Hamburger, V. & Hamilton, H. L. A series of normal stages in the development of the chick embryo. *Dev. Dyn.* **88,** 49–92 (1951).

39. Scaal, M., Gros, J., Lesbros, C. & Marcelle, C. In Ovo Electroporation of Avian Somites. *Dev. Dyn.* **229,** (2004).

40. Taelman, V. F. *et al.* Wnt signaling requires sequestration of Glycogen Synthase Kinase 3 inside multivesicular endosomes. *Cell* **143,** 1136–1148 (2010).

666   41.   Ohtsuka, T. *et al.* Visualization of embryonic neural stem cells using Hes
667   promoters in transgenic mice. *Mol. Cell. Neurosci.* **31,** 109–122 (2006).
668   42.   Aster, J. C. *et al.* Essential roles for ankyrin repeat and transactivation domains in
669   induction of T-cell leukemia by notch1. *Mol. Cell. Biol.* **20,** 7505–7515 (2000).
670   43.   Manceau, M. *et al.* Myostatin promotes the terminal differentiation of embryonic
671   muscle progenitors. *Genes Dev.* **22,** (2008).
672   44.   Schneider, C. A., Rasband, W. S. & Eliceiri, K. W. NIH Image to ImageJ: 25 years
673   of image analysis. *Nature Methods* **9,** 671–675 (2012).
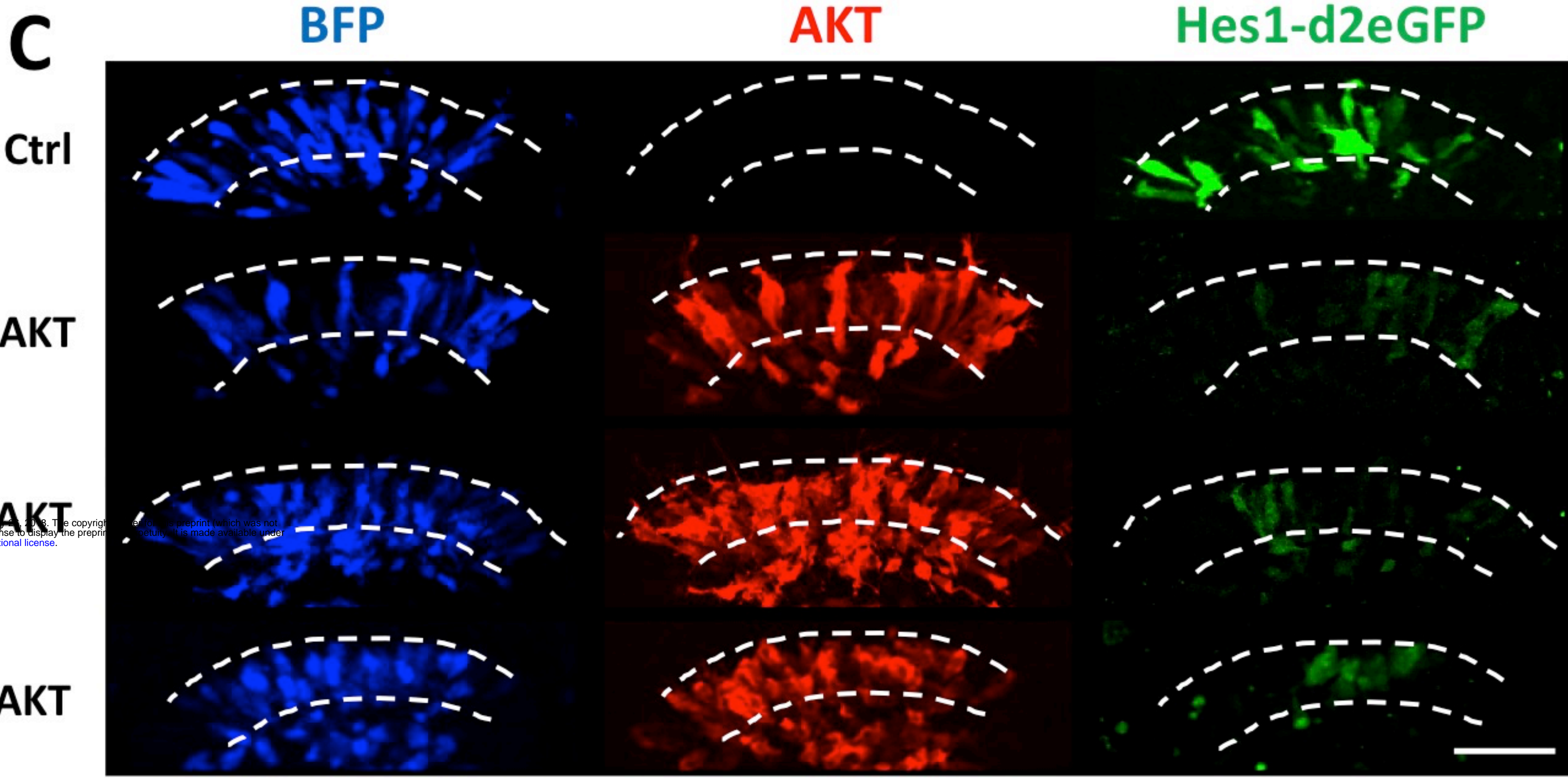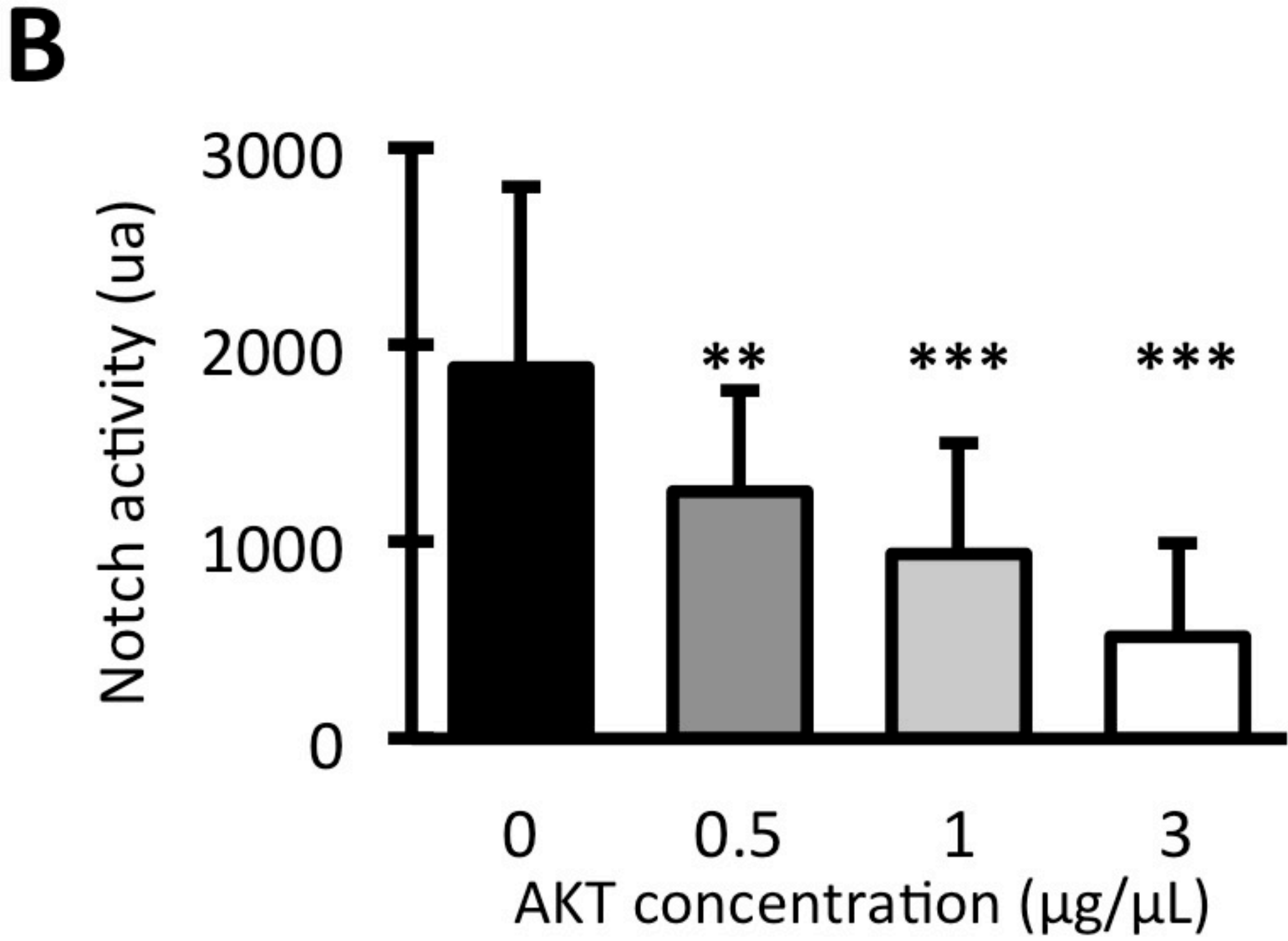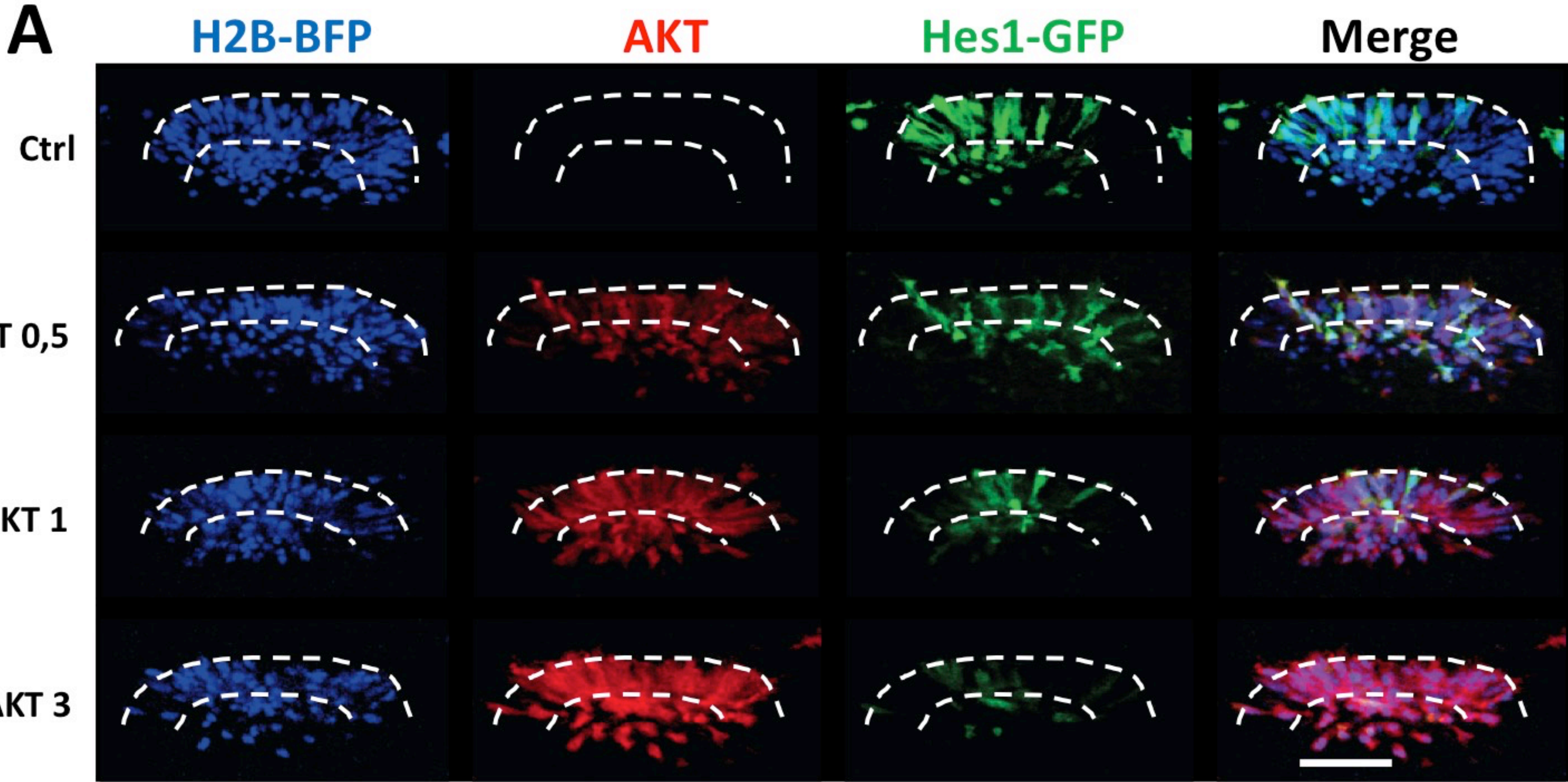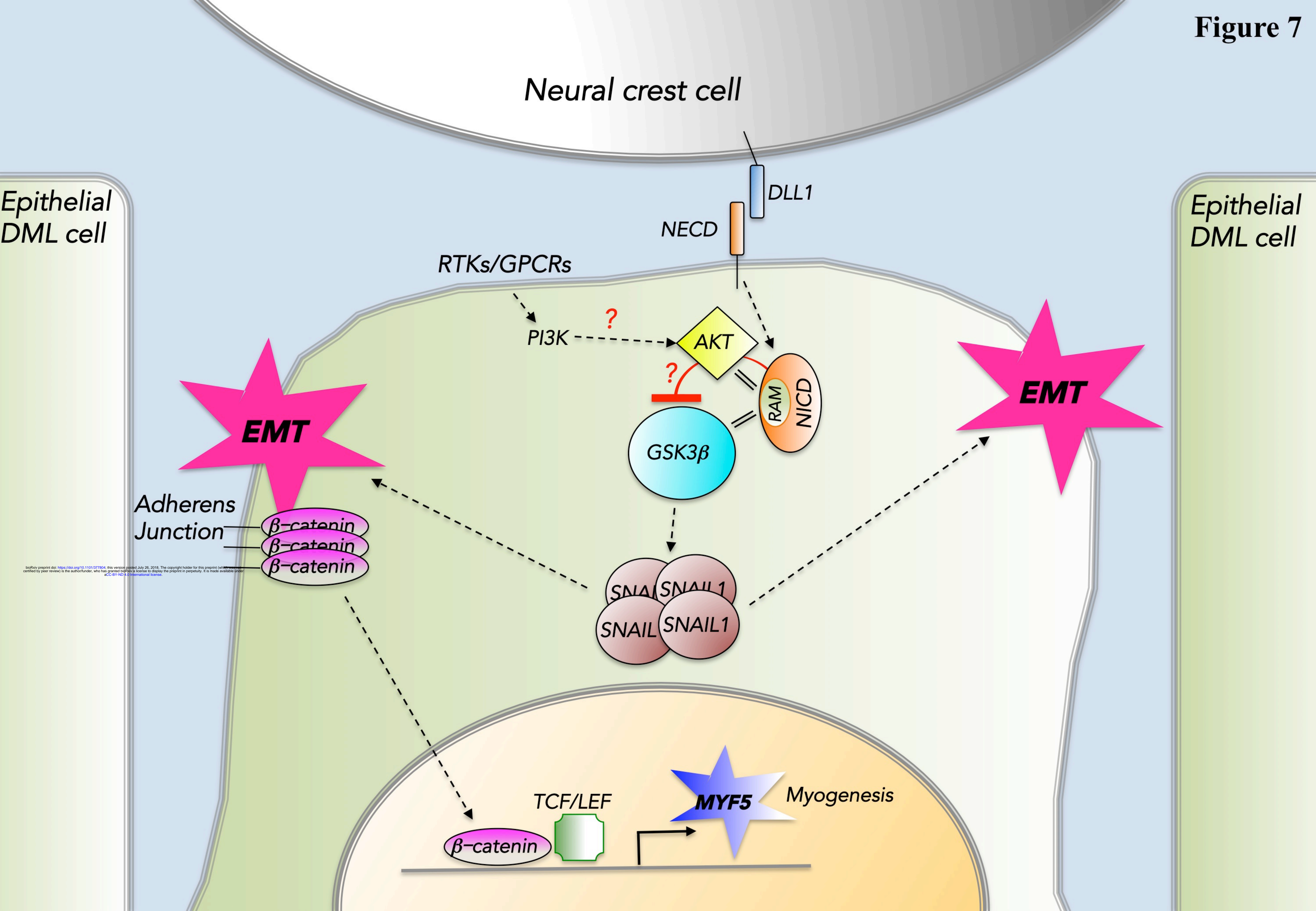674

Figure 1
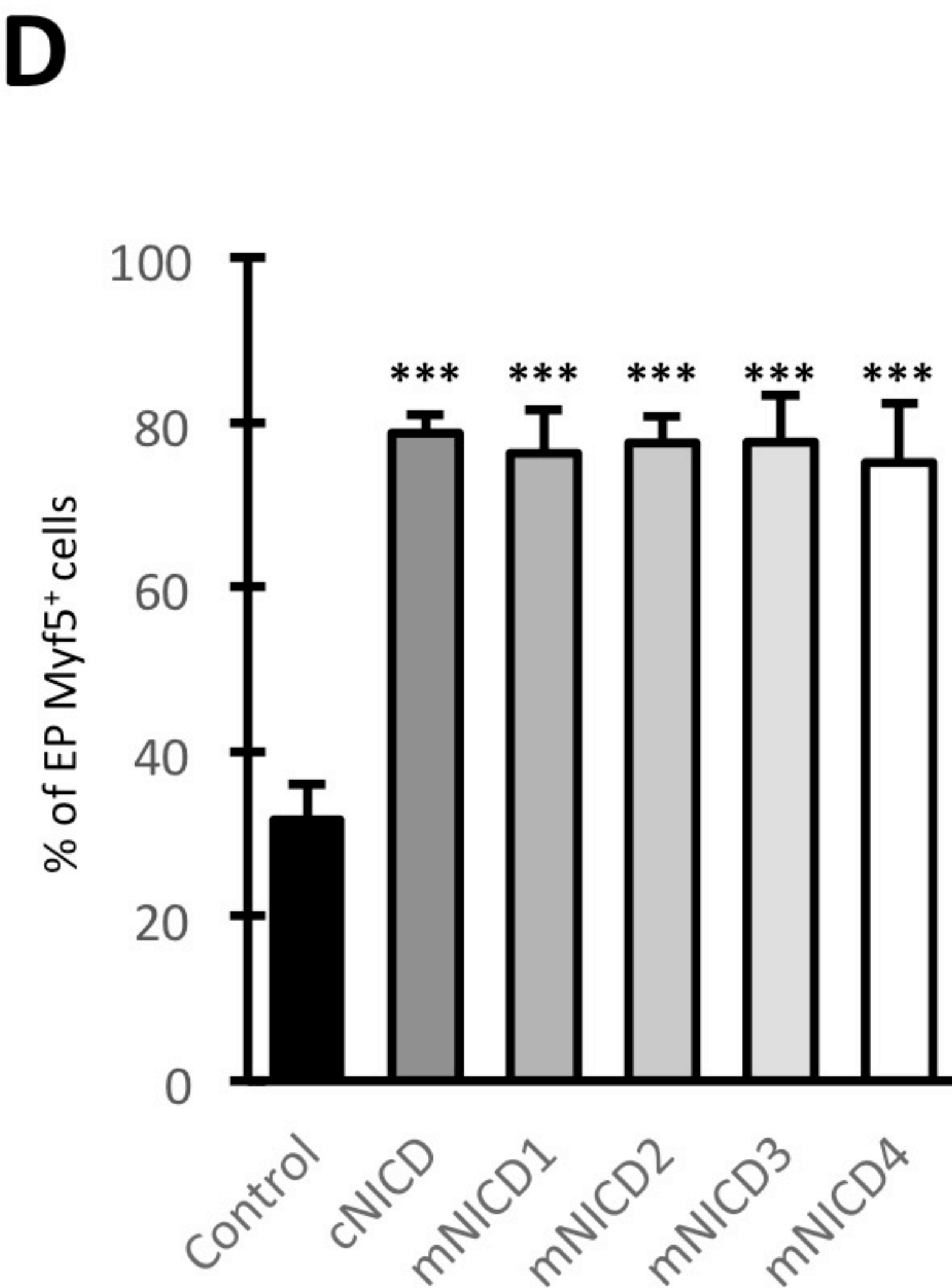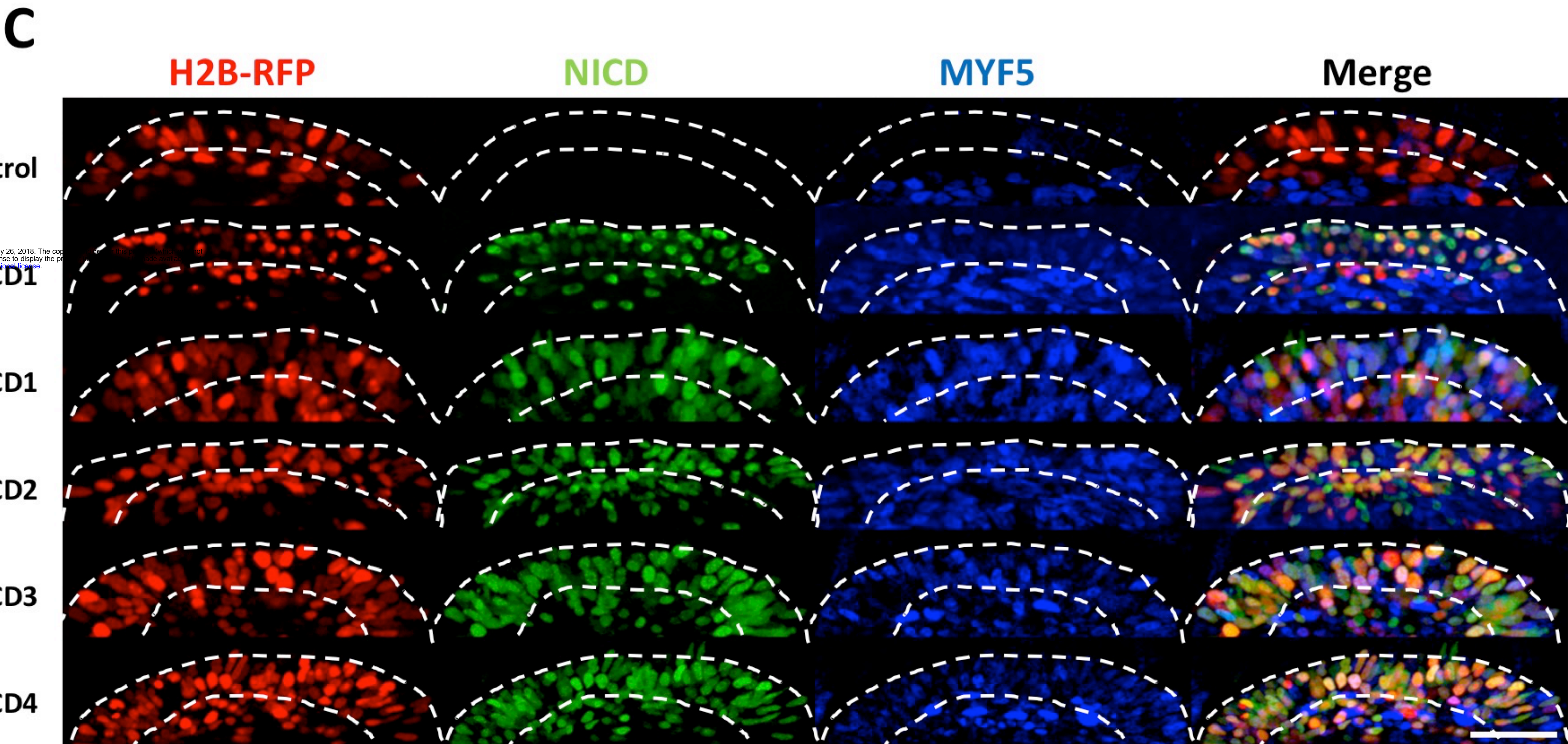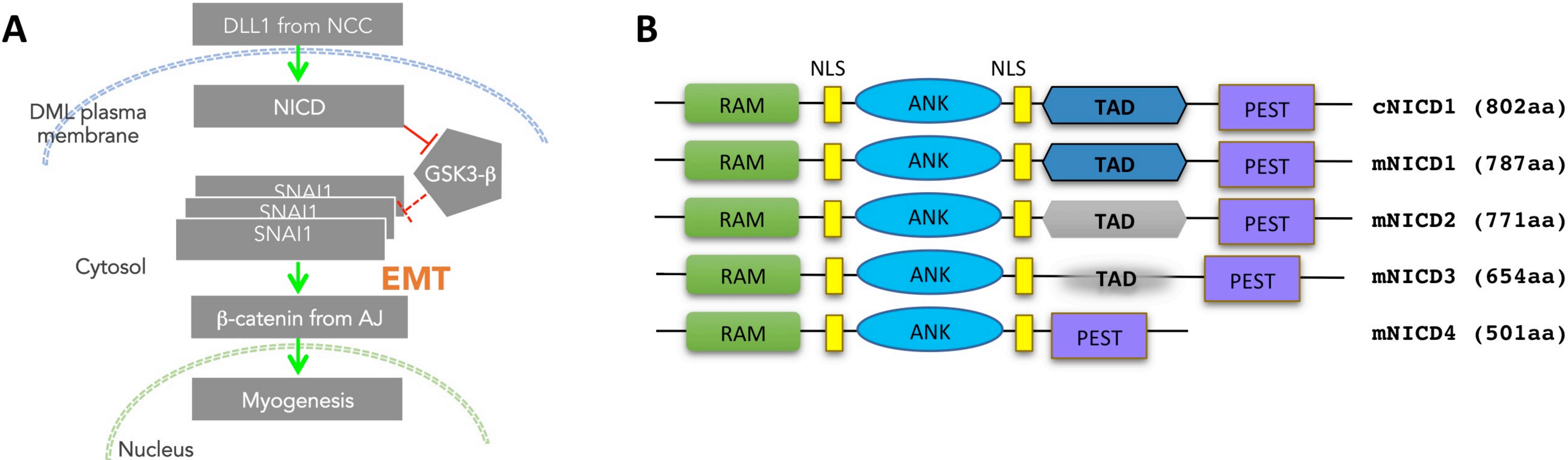
Figure 2
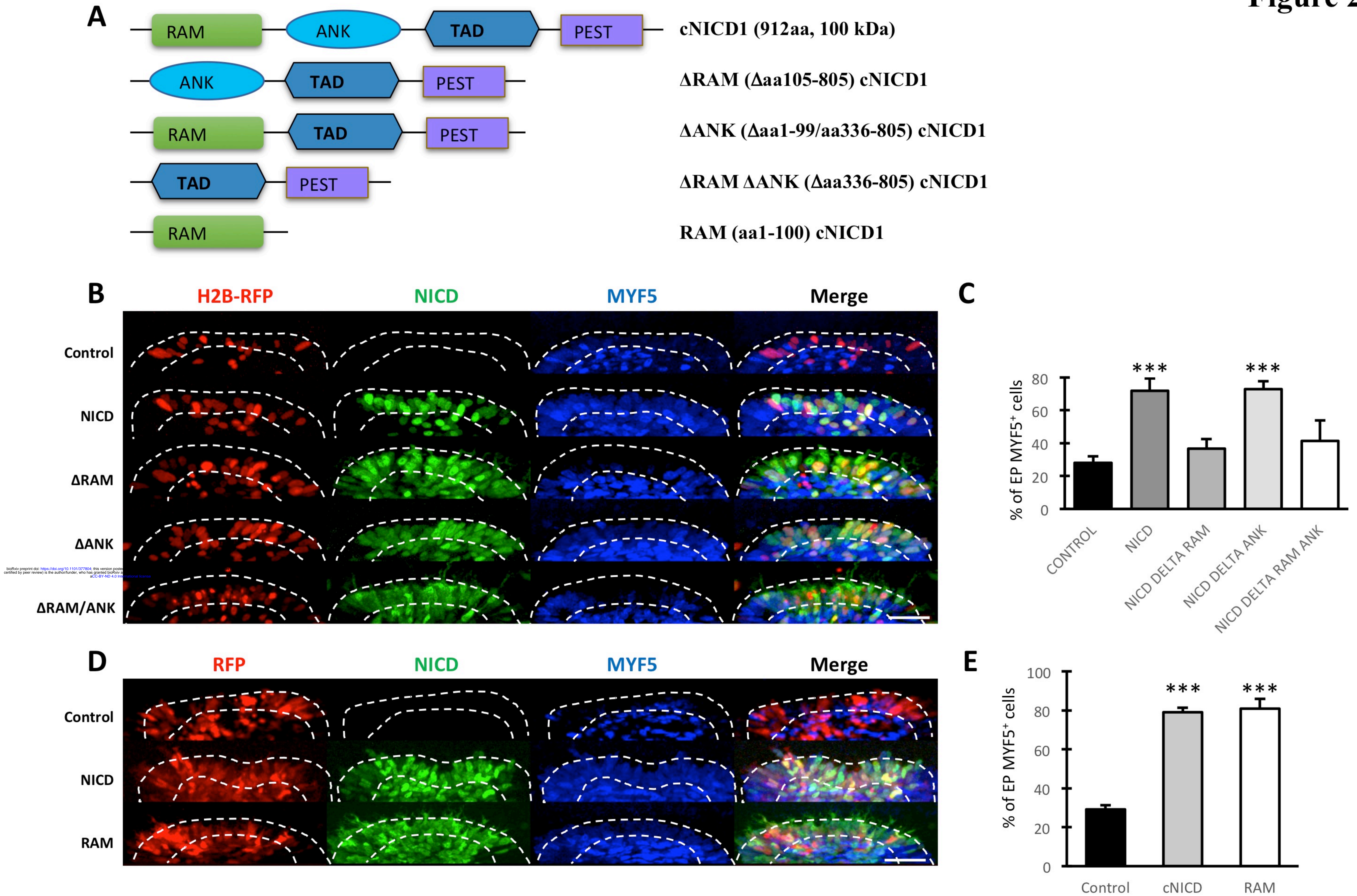
Figure 3

Figure 4

Figure 5

A
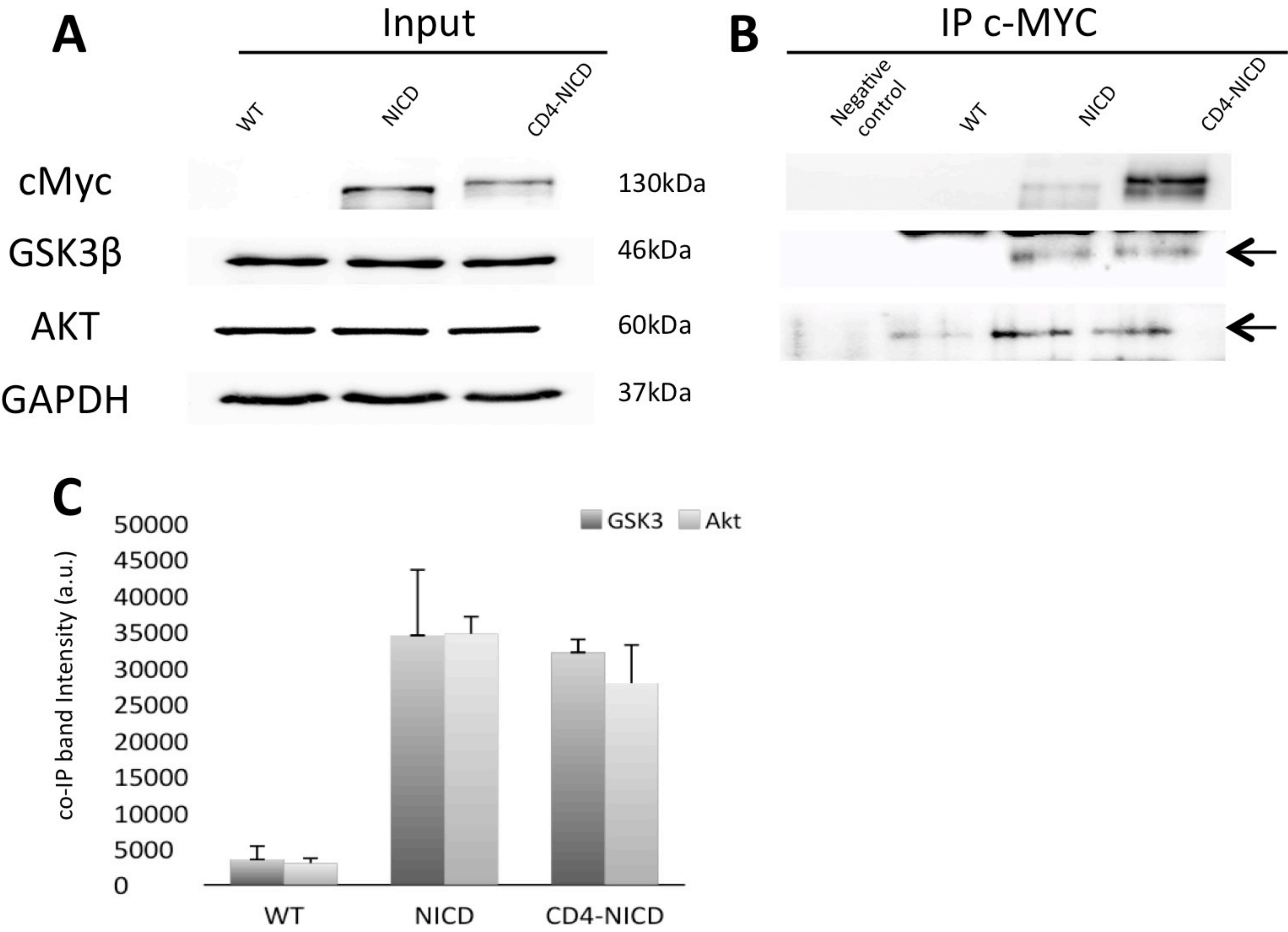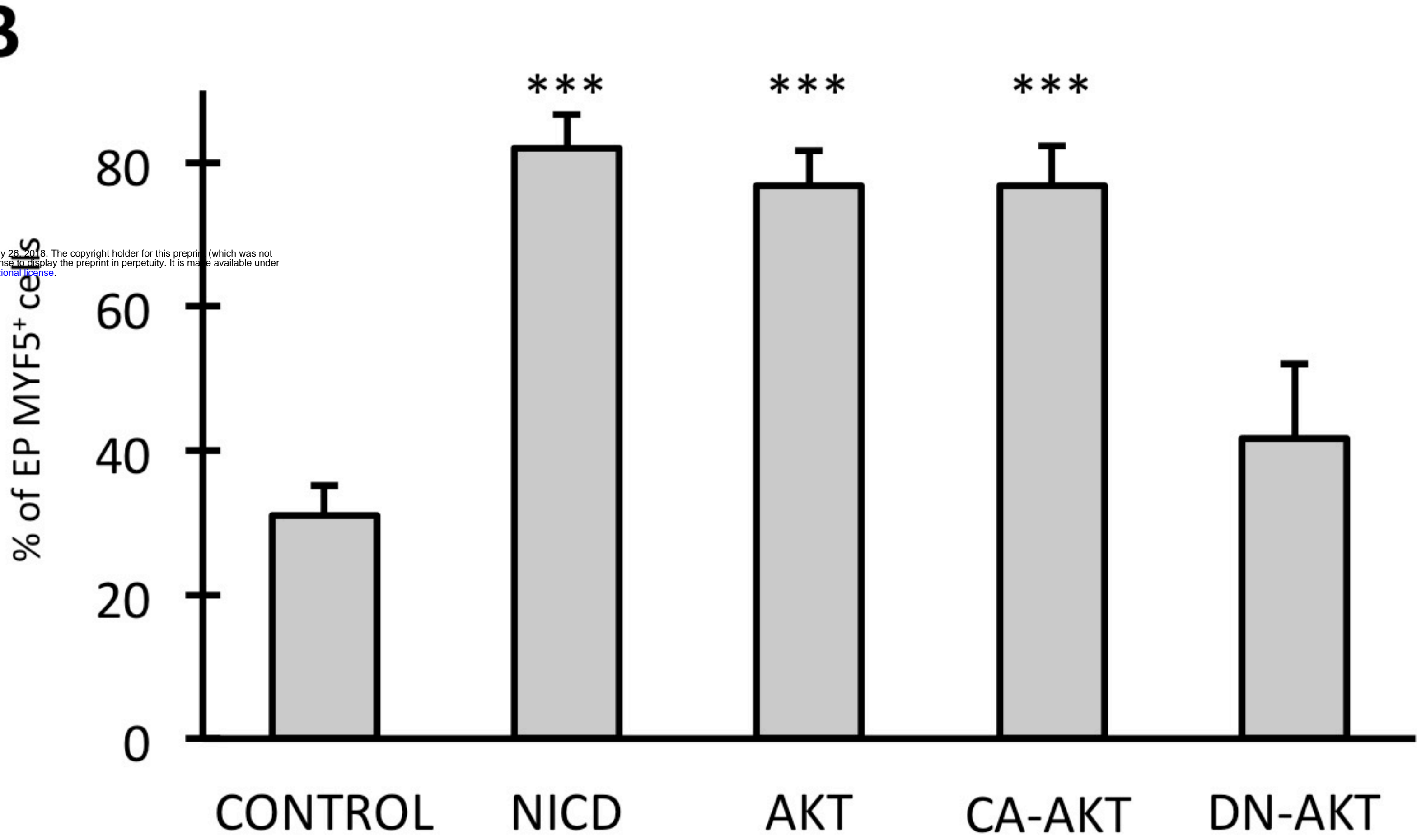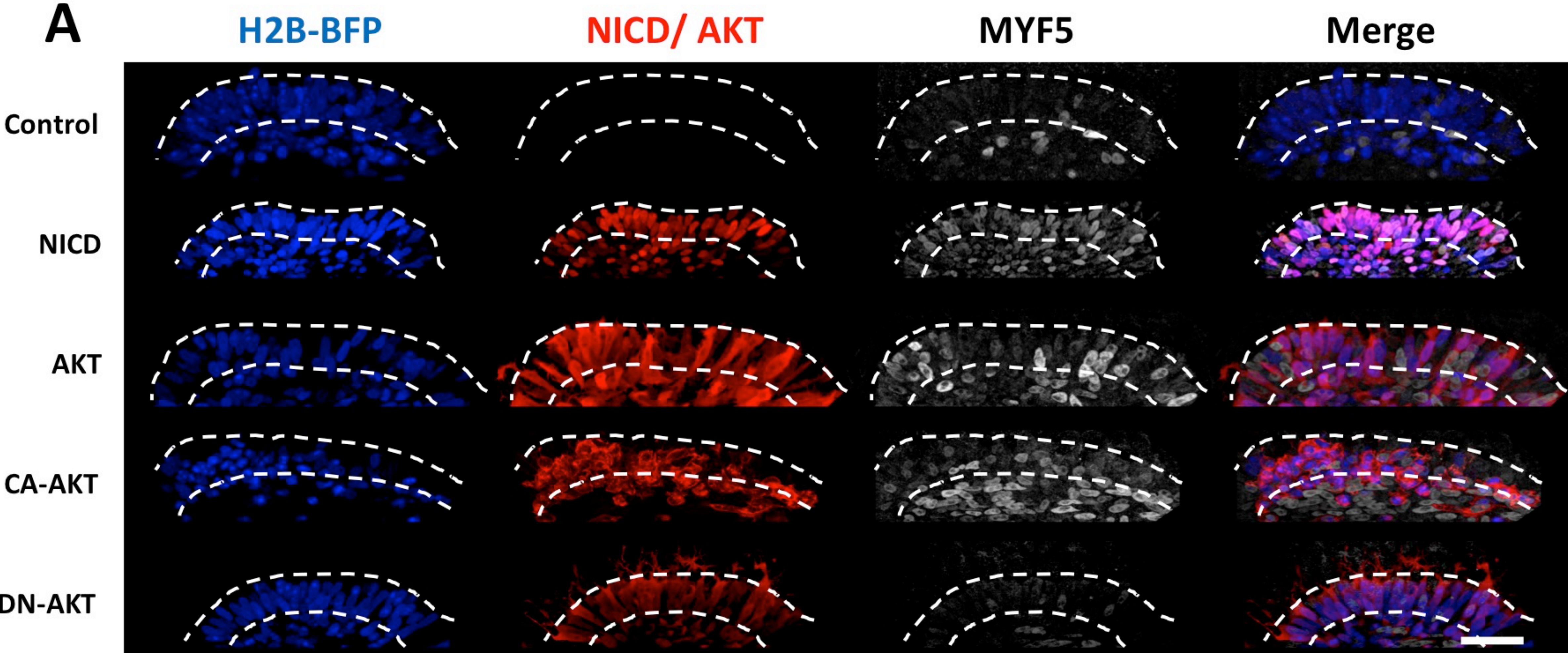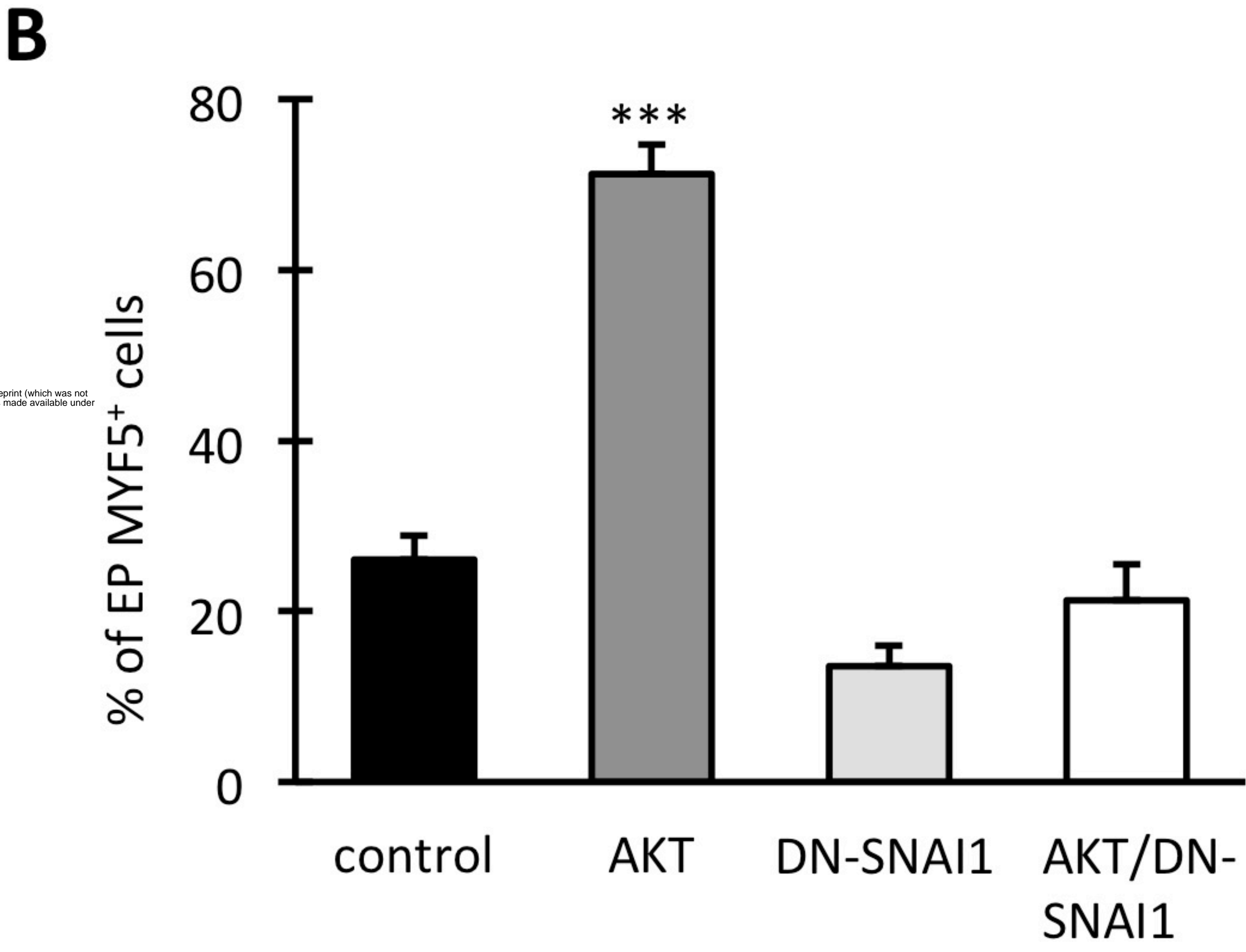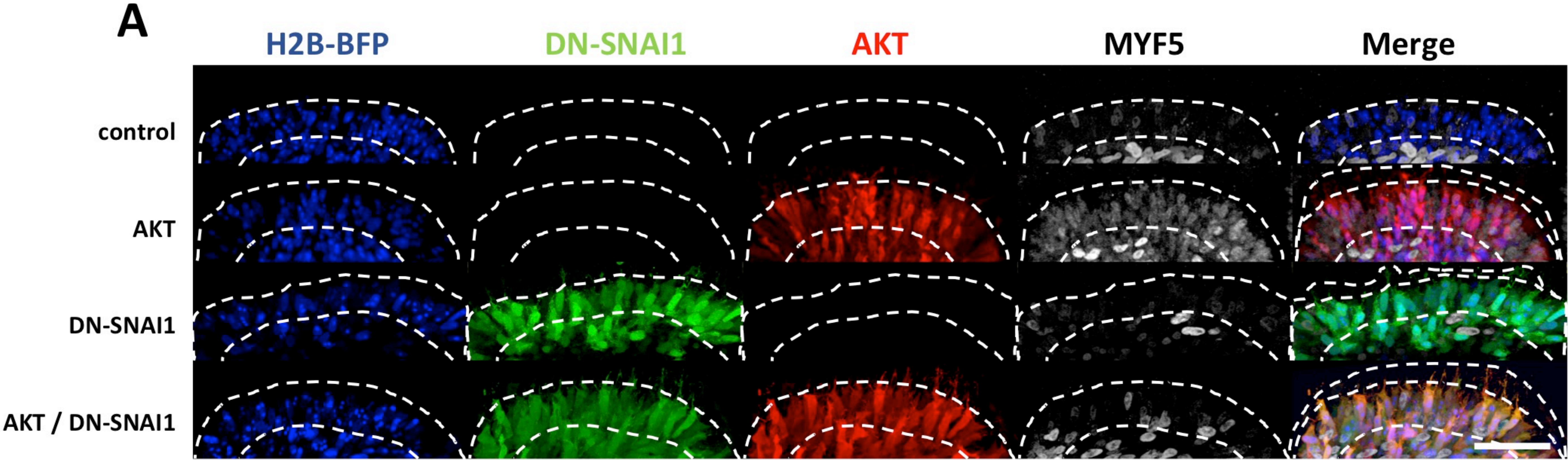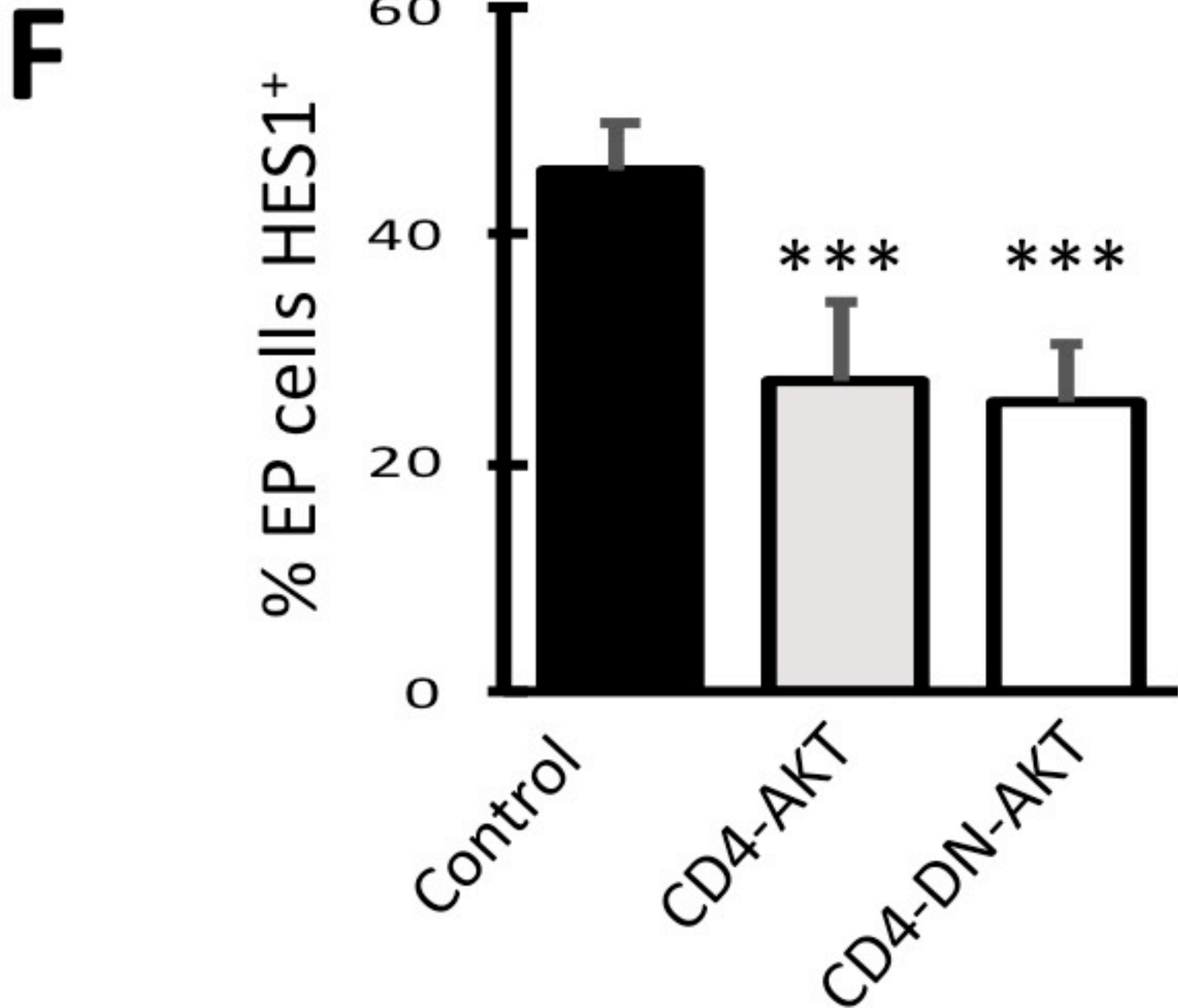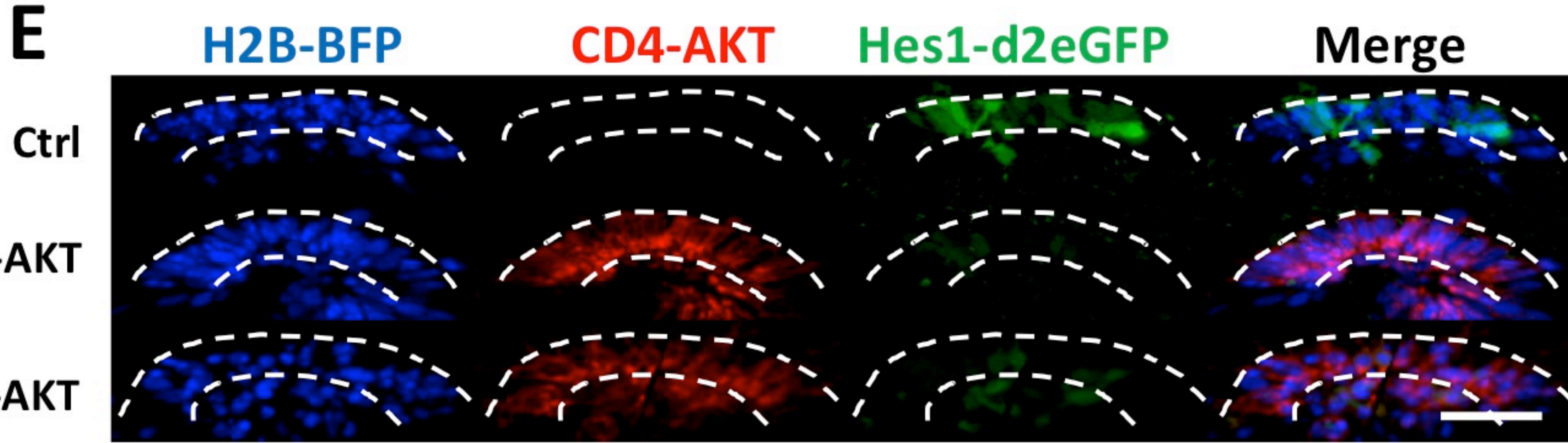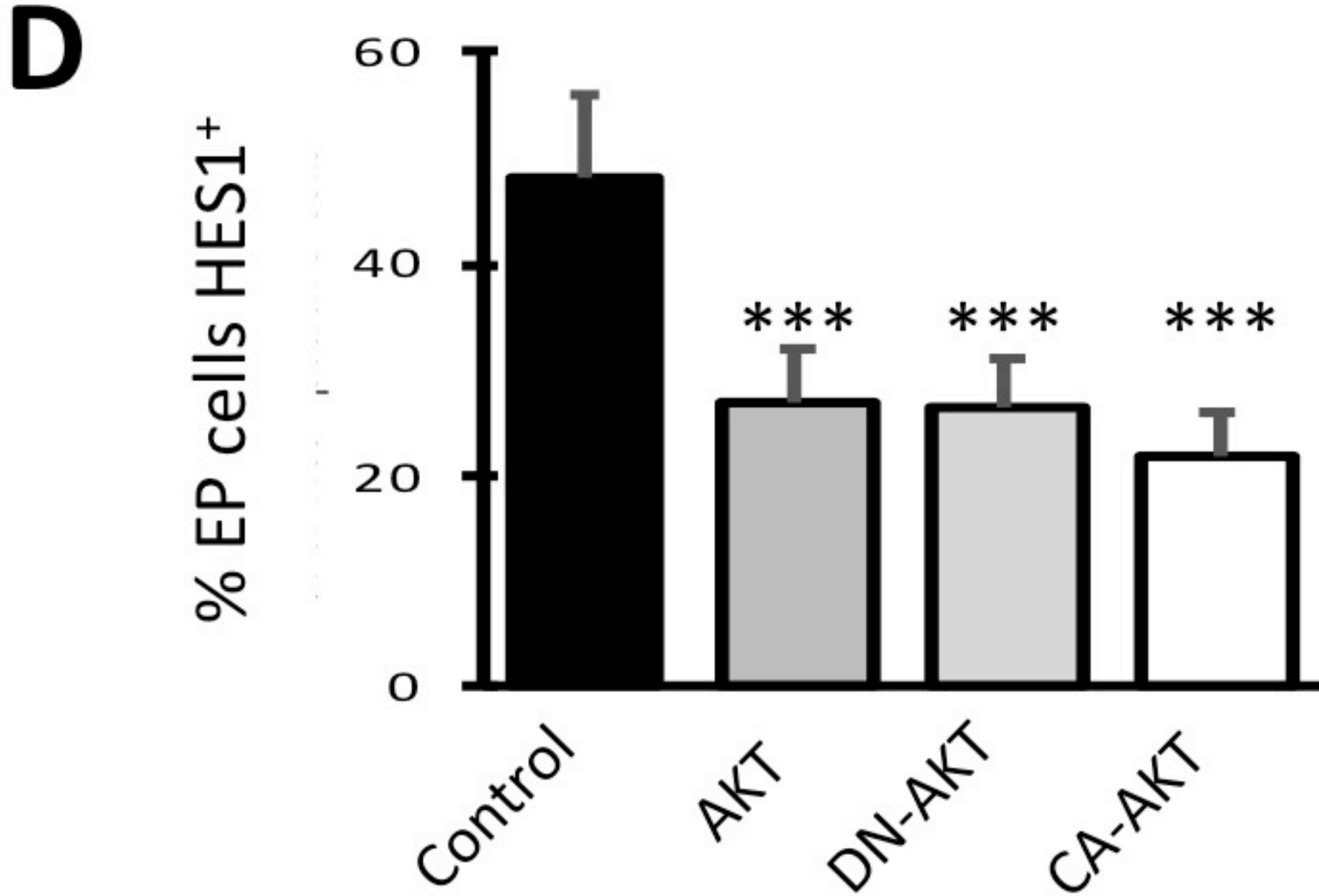
Figure 6

Figure 7

Figure 2 – figure supplement 1

Figure 3 – figure supplement 1